



Geospatially analysing the dynamics of the Khurdopin Glacier surge using multispectral and temporal remote sensing and ground observations

Muhammad Imran¹ · Umair Ahmad¹

Received: 19 November 2020 / Accepted: 17 March 2021 / Published online: 25 March 2021
© The Author(s), under exclusive licence to Springer Nature B.V. 2021

Abstract

Karakorum glaciers are well known for the advancement and the formation of new glacial lakes due to accelerated climate warming. Its Shimshal valley is profoundly affected by glacier surges in the last couple of decades. Khurdopin glacier is one of the highly surging glaciers in the Karakorum region. Its continuous surge since the nineteenth century is blocking the Shimshal River and creating new lakes. Our objective is to investigate the Khurdopin glacier surge from 1999 to 2017. With this, we aim to identify possible climate and topographic controls on the glacier surge behaviour. We used Landsat 4–5, 7 and 8 satellite bands and ground observations to estimate the glacier retreat and new land cover types from the glacier surge. Our results show that the Khurdopin glacier surges every 20 years. We observed the first surge of 0.69 Km² in 2000 and the second surge of 0.63 Km² in 2017. Both events blocked the Shimshal River. We observed an increase of 1–4 °C in the glacier minimum and maximum winter temperatures. Moreover, we observed snowfall variations in the accumulation zone in the steep glacier slope with a north slope-aspect. The 64% of the glacier aspect is north that causes an increase in ice mass in the accumulation zone by receiving more snowfall in the winter season. The study output, combined with earlier findings, can further predict a surge event in the future.

Keywords Glacier advancement · Climate change · Time-lapse image analyses · GIS · NDWI · NSDI

1 Introduction

Glaciers benefit millions of humans, biodiversity, and ecosystems through recharging the water reservoirs. Climate warming has caused significant glacial retreats and snowmelt in the Himala, the Karakorum, and Hindu Kush (HKH) region (You et al. 2017).

✉ Muhammad Imran
imran.igeo@uaar.edu.pk; ch.m.imran.sarwar@gmail.com

Umair Ahmad
umair444pk@gmail.com

¹ Institute of Geoinformation & Earth Observation (IGEO), PMAS Arid Agriculture University, Rawalpindi, Pakistan

As a result, the ever-increasing glacier lakes are evident in the region, both in terms of number and size (Rashid et al. 2020). Moreover, extensive road networks are recently built across significant glaciers in Pakistan under the China-Pakistan Economic Corridor (CPEC) initiative. Due to high freight volume, high CO₂ emissions will cause a rise in temperatures and ecosystems' degradation in the mountainous forests and glaciers (Nabi et al. 2018). With fully functional CPEC freight, an estimated 7,000 heavy vehicles will cross the glacier area per day, resulting in up to 36.5 million tonnes of CO₂ emissions. Such a high carbon release can accelerate snow-melting and new lakes in the HKH glaciers (Awais et al. 2019), which often results in massive water storage on the glacier's terminus. The water pressure often breaks the unbalanced moraine dams (Bajracharya et al. 2019). Thus a massive water discharge in a flash remains a natural hazard for life, infrastructure, farmlands, forests, and pastures downstream (Rashid and Majeed 2018).

Glaciers usually surge when the moraines cover holds back the ice discharge. The glacial flow in the HKH region was normal and usual at many sites until the nineteenth century. However, recent glacier advancements in the region may be attributed to several agents. Paul (2015) reported that heavy snowfall increased the ice mass in the accumulation zone of surging glaciers. Basal sheer pressure might be another agent to deform the glacier bed (i.e., thermal switch hypothesis) (Veettil et al. 2018). Quincey et al. (2011), Bhambri et al. (2020) found the water channel's breakage under a glacier may induce a hydrological switch. Besides, Sevestre and Benn (2015) investigated the glaciers' climatic and topographic traits to explain glacial surging behaviour. They conclude the precipitation and slope set up a primary control over the surging glaciers. Thus, to investigate a glacier advancement, the glacier's climatic and topographic attributes need to be linked with the earlier findings on other factors of the glacier surge (Fu and Zhou 2020). However, the annual and seasonal glaciological data is often scarce, which is the foremost hurdle to study the mass balance change and surges (Pfeffer et al. 2014; Quincey et al. 2015; Ashraf et al. 2017).

To investigate glaciers surge, field observations on the glaciological parameters are often time-consuming and labour-intensive to obtain, particularly in the large, inaccessible, and hazardous HKH region (Zhang et al. 2020). With a relatively small sample size, remote sensing (RS) has been widely used for glacier mapping due to the high spatial and temporal coverage of areal and space-borne sensors (Quincey et al. 2015; Rashid et al. 2018, 2020). However, the glacier debris cover poses challenges while estimating changes in the glacier mass balance and retreat over large areas. To this, a range of RS indices is developed by the multispectral image bands, such as Normalized Difference Water Index (NDWI) (Gilany and Iqbal 2020; Yan et al. 2020) and the Normalized Difference Snow Index (NDSI) (Racoviteanu and Williams 2012; Wang et al. 2015). They have been extensively used to monitor the hydro-meteorological limits of hazards like Glacial Lake Outburst Floods (GLOFs) (Bajracharya et al. 2019).

The present study investigates the Khurdopin glacier surge from 1999 to 2017 and estimates the glacier retreat and new land cover types from the glacier surge. With this, we aim to identify possible climate and topographic controls on the glacier surge behaviour. We used RS data with ground observations to derive several climatic and topographic variables and glacier land use land cover (LULC) classes (e.g., glacial lakes, debris). Furthermore, we derived indices from RS imagery to quantify the glacier water bodies and fresh snow. The study output, combined with earlier findings, can further predict a surge event in the future.

2 Materials and methods

2.1 Study area

Hunza district in Gilgit Baltistan is a glaciated region in Pakistan (Rashid et al. 2020). The district hosts hundreds of glaciers (USGS 2017), of which Khurdopin glacier is located at $36^{\circ}16'0''\text{N}$ and $75^{\circ}30'0''\text{E}$ (see Fig. 1). These glaciers are a source of freshwater (Awais et al. 2019). They play an essential role in the country's economy (Ashraf et al. 2017) and ecosystems maintenance (Nabi et al. 2018).

In October 2016, the Khurdopin Glacier surge accelerated after 20 years of slower onset phase. It is visible from the pair of ASTER images (Source: NASA-JPL (2018)) acquired on August 20, 2015, Fig. 1(b); and, May 21, 2017, Fig. 1(c) (white and dark grey areas show the river in the lower right of the imagery). By March 2017, the glacier moraine dam formed a large lake by blocking the Shimshal River. Before the catastrophic failure of the moraine dam burst the lake, the river created a terminal through the glacier.

The Khurdopin glacier surge is a constant risk for many sites linked with the glacier. The livelihood of the Shimshal valley critically depends on the glacier behaviour (Iturri-zaga 2005). Any change in the glacier dynamics may crucially affect the Shimshal River's hydrological systems (Hunza sub-basin) (Steiner et al. 2018). Furthermore, like a burst dam, the glacier surging can cause the glacial lake outburst where the large lake water abruptly floods down the valley. For instance, on 1 August 2017, the glacial lake outburst flood (GLOF) damaged the connecting roads between central Hunza and Shimshal valley. About six sites have been identified as a potential risk for developing similar threatening events in the Shimshal valley (Senese et al. 2018). The glacier surging and formation of glacial lakes hazards the people living in the plains downstream.

2.2 Data

2.2.1 Ground data

In this study, the LULC classification and other image analyses require ground observations for different control points on the Khurdopin glacier. For this, we randomly took 100 observations of the glacier's land use classes through GPS-based ground surveys, aerial photographs, and relatively high-resolution Google-Earth imagery. They were randomly split into two subsets, i.e., 70% for training the classifier and the other 30% to set the reference pixels for accuracy assessment. Furthermore, we interviewed the local communities about the past glacier surges and their effect on various LULC changes in the study area.

2.2.2 Satellite imagery

Table 1 summarizes the satellite imagery of Landsat 4–5 Thematic Mapper (TM), Landsat-7 Enhanced Thematic Mapper Plus (ETM+) for the years 2000 and 2010, and Landsat-8 (OLI+TIRS) for the years 2016 and 2017, acquired from USGS-EROS (<https://www.usgs.gov/>). Landsat-7 TM has seven bands covering wavelengths: 0.52–0.60 (Green), 0.63–0.69 (Red), 0.76–0.90 (Near Infrared), and 1.55–1.75 (Shortwave). Moreover, we

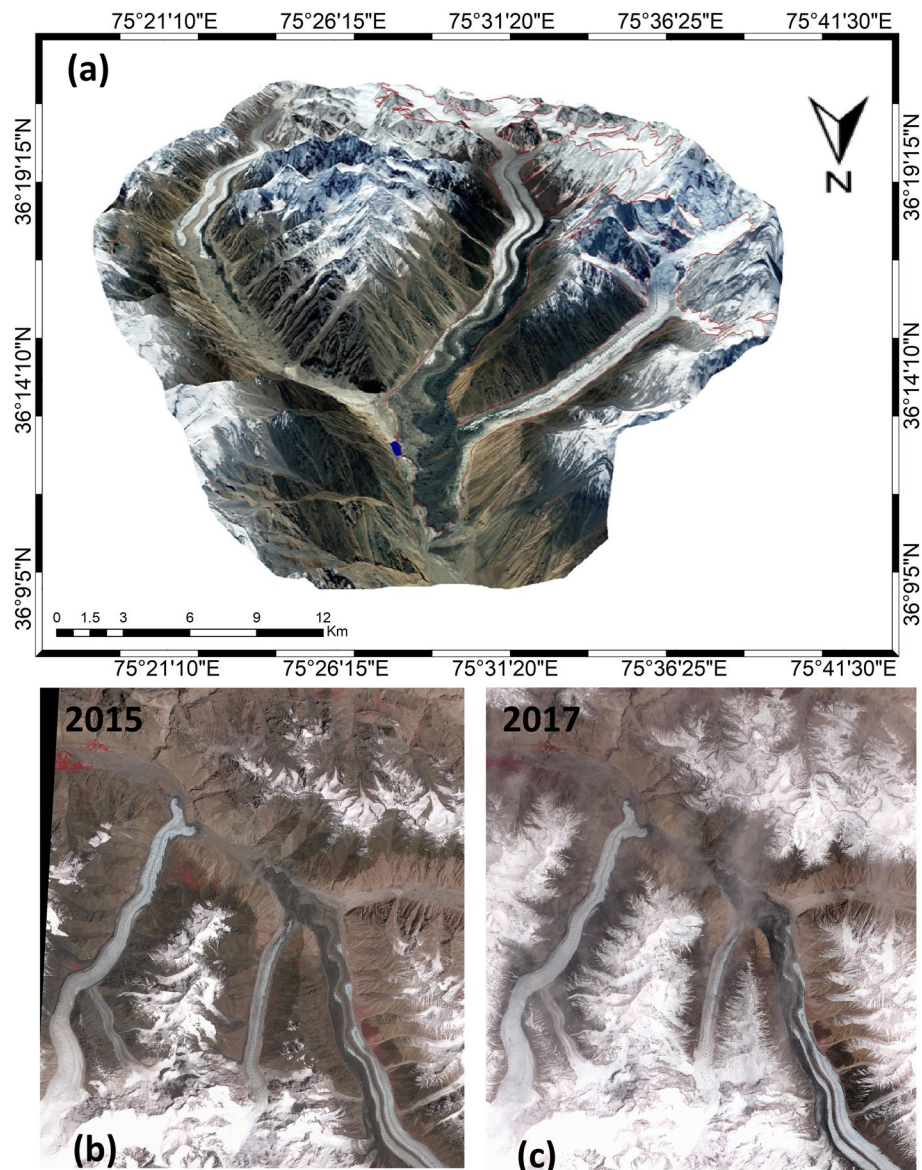


Fig. 1 A 3D view of the Khurdopin glacier (a), In the ASTER images acquired on August 20, 2015 (b) and May 21, 2017 (c) (Source: NASA/METI/AIST/Japan Space Systems, and U.S./Japan ASTER Science Team), the Khurdopin Glacier surge can be seen through comparing the before and after images. The study area covers an area of 25×27.8 km, and are located at 36.3° north, 75.5° east

used four spectral bands (i.e., Green, Red, Near Infrared, and Shortwave) with 30-m spatial resolution of the Advanced Space-borne Thermal Emission and Reflection Radiometer (ASTER) sensor.

To derive different land cover classes for the study area, we processed Landsat-7 images with 30-m ETM+ bands (1–5 and 7) and one thermal band with 60-m spatial resolution.

We used eleven Landsat-8 bands (i.e., 1–7 and 9 OLI bands, bands-8 panchromatic, and 10–11 thermal bands). The TM and ETM+ thermal bands have 120-m and 60-m spatial resolutions, respectively, but the USGS delivers those bands at 30-m after resampling through the cubic convolution algorithm (Jiménez-Muñoz et al. 2014; USGS 2017).

2.2.3 Topographic data

We aim to identify possible topographic controls on the surging behaviour of the Khurdopin glacier. For this, we downloaded the global high spatial resolution digital elevation model (GDEM) Version 2 from <http://gdem.ersdac.jspacesystems.or.jp/>, derived from 30-m ASTER (USGS 2017). This data set has been proved suitable to compile the glacier topographic parameters (Sevestre and Benn 2015) and to quantify climate variation in the HKH region (Gardelle et al. 2014). The DEM data were processed to create the slope and aspect surfaces for the Khurdopin glacier. Section 2.3. provides details on processing DEM data for this study.

2.2.4 Climatic data

We obtained the temperature and precipitation data from 21 weather stations in the region. For this, we downloaded 1999–2017—data freely from the Pakistan Meteorological Department (PMD) and the China Meteorological Administration (CMA) websites. Besides, we obtained the meteorological data from the high altitude stations operated by Pakistan's Water and Power Development Authority (WAPDA). These variables were interpolated using ordinary kriging to create the 30-m temperature and precipitation surfaces for the whole study area. Moreover, the satellite-derived precipitation data were downloaded from the IMERG Precipitation (3GPM_IMERG_v06) by Giovanni (<http://giovanni.gsfc.nasa.gov/giovanni>). We used this data set to calculate mean precipitation maps for the winter seasons from 1999 to 2017.

2.3 Methods

The workflow diagram in Figure 2 describes several methods applied in the present study.

We geo-referenced the imagery by the Universal Transverse Mercator (UTM) projection and applied radiometric calibration with band interleaved by lines format. Next, we performed the atmospheric correction to ASTER and OLI/Landsat-8 images: (i) to remove the effects caused by clouds and water vapours, and (ii) to convert the digital values to surface reflectance. For this, we used sensor altitude, sensor type, elevation, and multispectral settings in the FLASH (Fast Line of Sight Atmospheric Analysis of Hypercubes) module. To improve imagery visualization, we removed the Landsat imagery's noise errors in 2000, 2010, 2016, and 2017. These errors occur due to Scan Line Corrector's malfunctioning (SLC) of all Landsat 7 ETM+ imagery collected after May 31, 2003 (<https://landsat.usgs.gov/what-landsat-7-etm-slc-data>). We removed the scan lines from 2010 and 2017 satellite images using the ENVI "Landsat Gapfill" tool.

The Landsat data is often classified to identify the glacier surge events and resulting land cover changes in space and time (Fayaz et al. 2020). We used the maximum likelihood (ML) method for the supervised LULC classification of the Khurdopin glacier. For this, we collected signatures for different land cover types from on-ground training sites. We used ArcGIS to train data after stacking the calibrating bands in SWIR2 (7), NIR (4), Green (2)

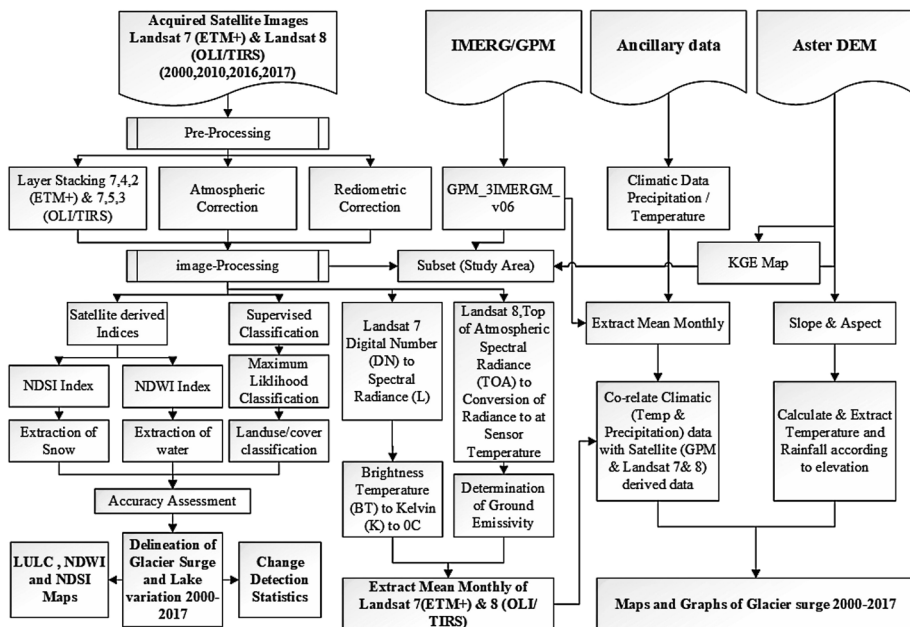


Fig. 2 Flow chart shows processing and methods used in the research

(2000 and 2010 Landsat 7 ETM+ imagery), and SWIR2 (7), NIR (5), Green(3) (Landsat 8 (OLI+TIRs) 2017 image). Overall accuracy of ML is higher compared to that of other methods, provided that samples are normally distributed in study area Ge et al. (2018). In this study, we used a single threshold value with the 1.0 data scale factor.

For the years 2000, 2010, 2017, we used the Normalized Difference Water Index (NDWI) to map the glacial lake variations and the Normalized Snow Difference Index (NSDI) to quantify the temporal change of snow cover and glacier cover (explained in the following sections). The raster surfaces from the LULC classification and the indices normalization were converted into the vector format to calculate areas for different land cover types of the Khurdopin glacier. We compared the spatial and temporal variations in those land cover types to better understand the glacier surge behaviour. Next, we calculated the glacier surge volume and the glacier lake volume using the Surface Functional Volume tool in the ArcGIS environment. To do so, we used a combination of DEM and surged-glacier surface boundary and glacial lake outline.

The glacier slope and aspect surfaces can be investigated with other factors to explain the glacier melting and formation of new glacier surface lakes (Sevestre and Benn 2015). The melted water intrudes in the glacier surface bed. This melted water acts as a lubricant and causes surges and advancement of glaciers. We used the glacier slope and aspect maps to identify potential locations for the Khurdopin glacier advancement in the accumulation and ablation zones. We derived the glacier slope map from the DEM data to link the glacier advancement to different slopes. Similarly, we prepared the aspect map to identify the potential areas on the glacier surface where high solar radiation strikes.

We prepared temperature and precipitation surfaces to evaluate the climatic variations and their impacts on the Khurdopin glacier. To do so, we applied the Inverse Distance Weighted (IDW) method to interpolate climate data from ground meteorological stations.

IDW depends on the selection of the search neighbourhood strategy. We used a moderate weighting value of 4 with a radius of 3000 m in the interpolation. The land surface temperature (LST) often causes spatiotemporal changes on the glacier surface. We mapped the LST of the Khurdopin glacier using the thermal band of Landsat imagery to investigate this. The satellite-derived LST was correlated with the data from the ground-based meteorological stations. All maps were prepared in the ArcGIS environment.

2.3.1 Extraction of water bodies and snow cover areas

Normalized Difference Water Index (NDWI) is widely used to map water bodies like glacier lakes (Yan et al. 2020). To identify the temporal changes in the glacial lake, we calculated the NDWI surface of the study area, as

$$\text{NDWI} = \frac{(B_{\text{Green}} - B_{\text{NIR}})}{(B_{\text{Green}} + B_{\text{NIR}})} \quad (1)$$

The Normalized Snow Difference Index (NSDI) is often used to map the glacier snow cover (Wang et al. 2015). The NSDI surface for the study areas was calculated, as

$$\text{NSDI} = \frac{(B_{\text{Green}} - B_{\text{SWIR}})}{(B_{\text{Green}} + B_{\text{SWIR}})} \quad (2)$$

where characteristics of spectral reflectance from the near-infrared (NIR) to the short-wave-infrared (SWIR) make water and snow bodies distinguishable from other landscape features.

The NSDI surface was combined with the LULC surface to delineate the glacier land cover classes, i.e., snow cover and glacier cover. These surfaces were transformed into vector polygons, and the areas of the corresponding classes were calculated.

2.3.2 Extraction of land surface temperature

For August 2000 and 2017, we derived the LST surface for the Khurdopin glacier from the Landsat-7 (ETM+) imagery following the procedure, as described by (Chander et al. 2009). The extracted radiance values were then used to derive the satellite brightness temperature (i.e., blackbody temperature), followed by the correction for spectral emissivity according to the nature of the landscape (Weng et al. 2004). LST maps with band TI (6) (Landsat-7 ETM+), band TIRS2 (11) (Landsat-8), and top of atmosphere brightness temperature values were expressed in Kelvin (for details Imran and Mehmood 2020, pp. 5).

2.3.3 Accuracy assessment and validation

We developed LULC maps by classifying the Landsat imagery of the glacier retreat through randomly observed points on different LULC classes. The reference pixels we obtained from the GPS-based ground control points. However, for inaccessible terrains, water and ice bodies were marked through RS-derived indices (i.e., the NDWI and NSDI). The values of these points we further verified using visual interpretation and expert knowledge. For this, these points were converted into the KML format and overlaid on Google Earth. The reference points we randomly split into two subsets, a subset of 70% observations to train the classifier and a 30% subset for the validation purpose.

3 Results

Figure 3(a–c) shows the Khurdopin glacier surge and variations between 2000 and 2017. It indicates the formation of glacier lakes in the years 2000 and 2017 with the blockade Shimshal River. The glacier blockage area in 2000 was 0.69 km^2 while the glacial lake covered area was 0.52 km^2 . The glacier blockage area in 2017 increased to 0.62 km^2 with the glacial lake area equal to 0.38 km^2 . Figure 3b represents the surface area of the Khurdopin glacier in 2000, 2010, and 2017 having an area of 49.8 Km^2 , 46.2 Km^2 , and 49.06 Km^2 , respectively. The total area of the glacier was maximum in 2000 compared to 2010 and 2017. Our results confirm the local community perceptions about surging behaviour in the past, i.e., during 1960, 1980, 2000, and 2017, and findings from Steiner et al. (2018).

3.1 Khurdopin Glacier advancement from 2016 to 2017

To analyse the latest glacier surge in 2017, Figure 4a–d shows the status of the Khurdopin glacier from October 2016 to November 2017. Figure 4a indicates no lake on 28 October 2016, and we were unable to observe the glacier surge. On 23 May 2017, the glacier surge seen in Figure 4b surged and blocked the Shimshal River, and, consequently, a lake was formed. From 28 October 2016 to 23 May 2017, due to the Khurdopin glacier surge, the river blockage length equals 962.57 m^2 . For the same period, the glacier surge area was $270,000 \text{ m}^2$ that produced total glacial deposits equal to $6257688.99 \text{ cubic meters}$. Glacial depositions occur after settling sediments left behind by a moving glacier. Through carefully examining this from the time series of Landsat imagery, we found a build-up phase before the current surge, which distinguishes the surging behaviour from an avalanche.

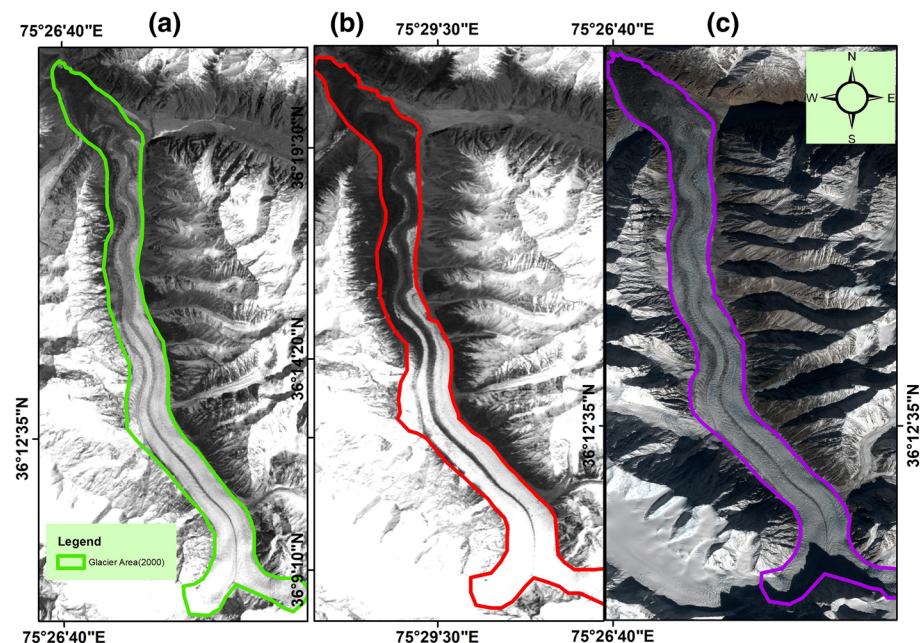


Fig. 3 Khurdopin glacier area in the years 2000 (a), 2010 (b), and 2017 (c)

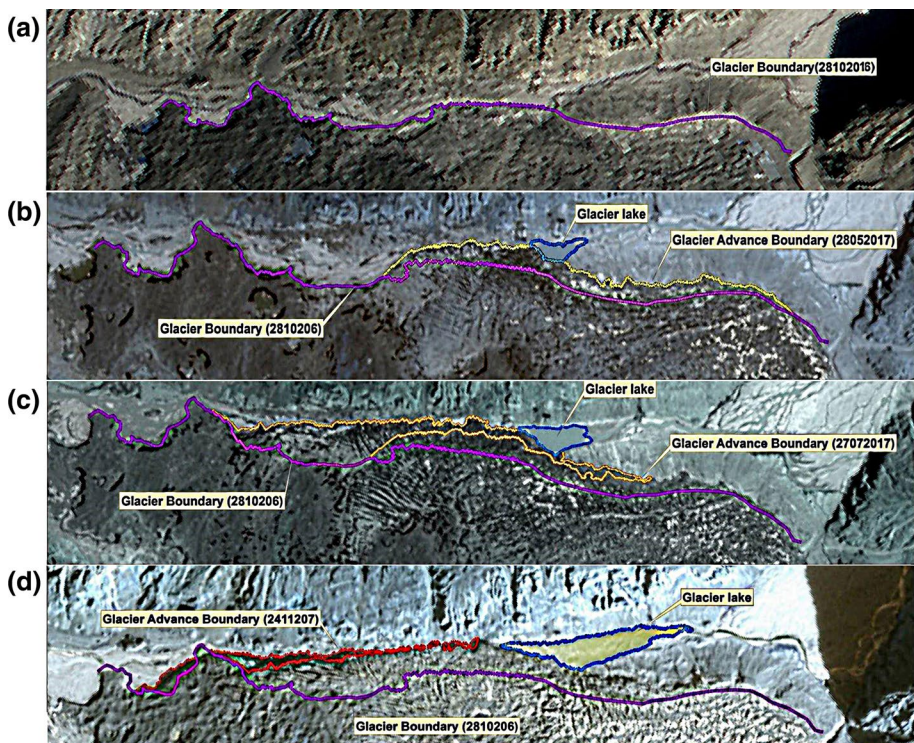


Fig. 4 Spatial and temporal variations of the Khurdopin glacier on October 28, 2016 (no lake formed) (a), May 23, 2017 (b), July 27, 2017 (c), and November 24, 2017 (d)

On 27 July 2017, the glacier surge advanced to increase the lake area (see Fig. 4c). From 23 May to 27 July 2017, the length of the river blockage increased to 1998.54 m^2 . For this period, the glacier surge area was $340,000\text{ m}^2$ that produced total glacial deposits equal to 16656060.02 cubic meters.

On 24 November 2017, the Khurdopin glacier further advanced to increase the area of the lake to a maximum (see Fig. 4d). From 27 July to 24 November 2017, the river blockage increased with a length of 364.81 m^2 leaving the total blockage length to 2363.35 m^2 . For this period, the glacier surge area was 100000 m^2 that produced total glacial deposits equal to 863416.61 cubic meters. Thus, from 28 October 2016 to 24 November 2017, we observed a glacial surge of 710000 m^2 .

3.2 Khurdopin glacier lake variations

Figure 5(a–f) shows the Khurdopin glacier lake variations during the glacier surge from October 2016 to December 2017. No glacier lake is seen on 28 October 2016 in Fig. 5a. The glacier surge starts in 2017 that blocked the Shimshal River. On 23 May 2017, the glacier lake covers the area of 2.72 ha (Fig. 5b). On 27 July 2017, the glacier lake covers the area of 5.36 ha (Fig. 5c). The glacier lake area increases on 24 November 2017 and covers the area of 14.80 ha (Fig. 5d). On 27 December 2017, the glacier lake area increases to a

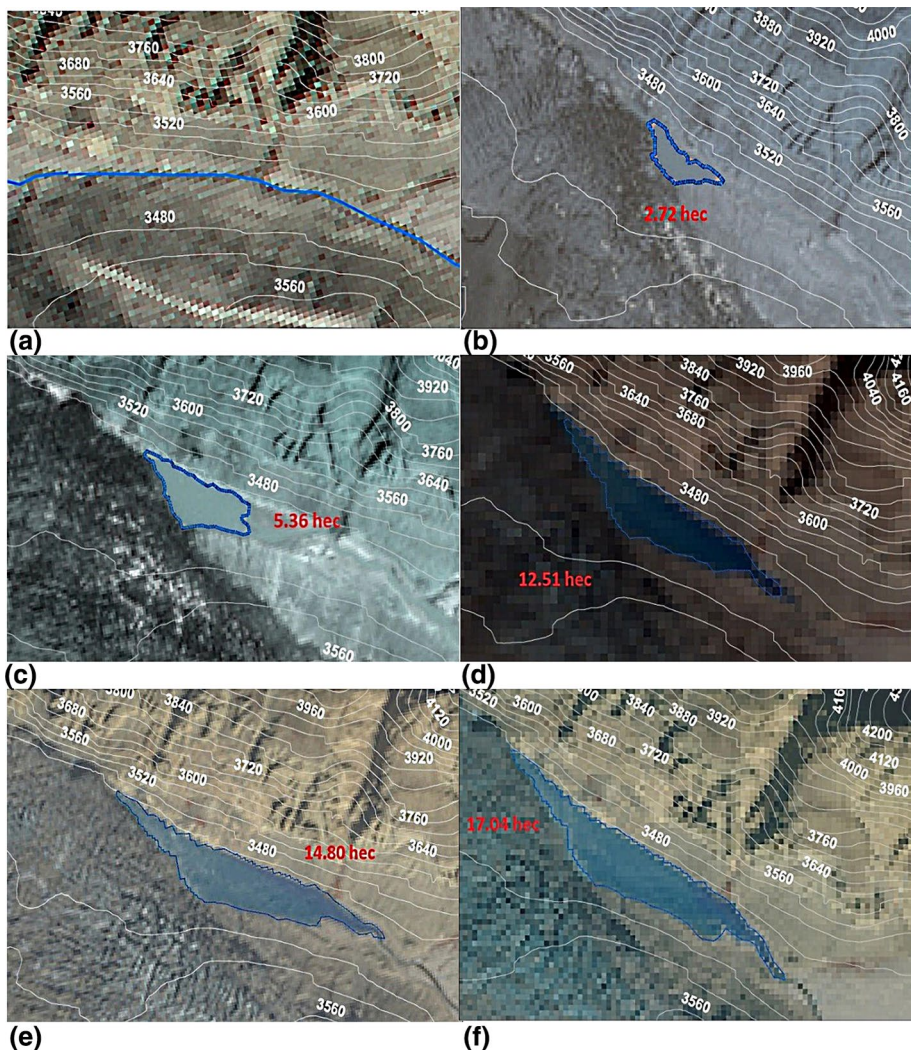


Fig. 5 Spatial and temporal variations of the Khurdopin glacier lake on October 28, 2016 (no lake seen) (a), May 23, 2017 (2.72 ha) (b), July 27, 2017 (5.36 ha) (c) November 21, 2017 (12.51 ha) (d), November 24, 2017 (14.80 ha) (e), December 27, 2017 (17.04 ha) (f)

maximum of 17.04 ha (Fig. 5f). Our RS-derived measurements are in line with the photographs taken by FOCUS geologists during Hali surveying in 2017.

3.3 LULC map for the year 2017

Figure 6a shows the LULC map of the Khurdopin catchment classified from the ML classification. Figure 6b shows areas of the glacier LULC classes. It indicates the glacier snow area covers 157 Km², the glacier debris covers an area of 54.24 Km², and the area covered by water bodies is 0.10 Km². The LULC map of the glacier watershed helped analyse the

Table 1 Test results for convergent validity in the outer model

Data	Acquisition date	Path	Row	Spatial res.	Temporal res.	Source	Uses
Landsat 7 (ETM+)	17-04-2000	149	35	30-m	16days	USGS	LST & LULC
Landsat 7 (ETM+)	15-04-2010	149	35	30-m	16days	USGS	LST & LULC
Landsat 8 (OLI+TIRs)	28-10-2016	149	35	30-m	16days	USGS	LST & LULC
Landsat 8 (OLI+TIRs)	23-05-2017	149	35	30-m	16days	USGS	LST & LULC
Landsat 8 (OLI+TIRs)	27-07-2017	149	35	30-m	16days	USGS	LST & LULC
Landsat 8 (OLI+TIRs)	24-11-2017	149	35	30-m	16days	USGS	LST & LULC
ASTER	11 Nov 2010	—	—	30-m	—	USGS	Slope & Aspect
Climatic data	(2000-17)	—	—	—	Monthly	PMD	Temp & Perc
IMERG/GPM	2000-17	—	—	0.1°	Monthly	IMERG	Precipitation
Field data	2017	—	—	—	Yearly	FOCUS	Glacier Photo-graphs

snow accumulation rate on top of the glacier. The winter snow accumulation increases the glacier mass in the accumulation zone. Consequently, heavy ice mass and gravity cause the glacier to surge downstream.

Table 2 shows the user's and the producer's accuracy statistics. The overall accuracy of the classification is 90.25%. The kappa statistics for the classified LULC maps for the year 2017 is 0.891. The glacier and mountains/barren land classes have 83.33% and 91.52 % user's accuracies, respectively, and 83.33% and 88.23% producer's accuracies, respectively. The user's and the producer's accuracies of the water class, which is the main glacier class related to the formation of the glacial lake, are 98.00% and 90.45%, respectively. Among the glacier LULC classes, the snow class has 94.00% and 88.12% user's and producer's accuracies.

3.4 Variation in the Khurdopin glacier debris cover, snow cover, water bodies from the year 2000 to 2017

The maps in Fig. 7a–b delineate the spatial and temporal variations of fresh-snow cover (green) and debris cover (grey) of the Khurdopin glacier between the years 2000 and 2017. In the year 2000, the area covered by the debris glacier was 15.4 Km² while the fresh-snow covered area was 32.4 Km². In 2017, the glacier debris covered an area equal to 16.3 Km², and the area covered by the fresh-snow glacier was 31.9 Km². The fresh-snow cover decreased from 2000 to 2017, which gave rise to debris cover and the water bodies (i.e., in the form of glacial lakes); see NDWI maps for the same period in Fig. 7c–d). Through the NDWI maps with the LULC map for the year 2017 (Fig. 6), we observed that the water bodies over the glacier cover vary with vegetation cover and soil types of the glacier surface. The majority of glacial lakes or water bodies exist near the 255 DN value, while a DN value near 0 resembles vegetation features.

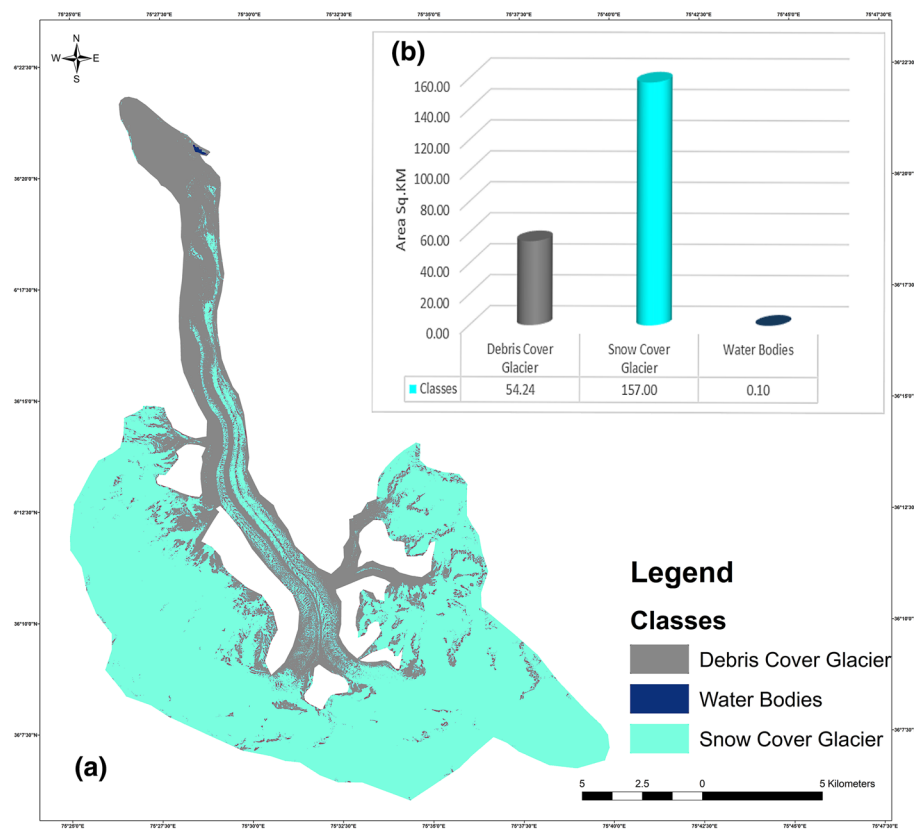


Fig. 6 Land use land cover (LULC) map of the Khurdopin catchment using maximum likelihood supervised classification

In the following sections, we investigated the glacier climatic and topographic variables that may cause the spatial and temporal variations in the Khurdopin glacier debris cover, snow cover, water bodies from 2000 to 2017. Investigating these variables with other factors would help better understand the surging behaviour of the Khurdopin glacier (Steiner et al. 2018).

3.5 Topographic variables of the Khurdopin glacier

Figure 8a shows the spatial variations of slopes over the Khurdopin glacier, which is a vital topographic parameter responsible for the movement of glaciers. The glaciers having lower slopes generally tend to surging (Sevestre and Benn 2015). We converted the slope raster into polygons to find the glacier areas in different slope intervals. The first slope interval (0–5.6 degrees) covers an area of 26.85 km², the second slope interval (5.6–10.6 degrees) covers an area of 22.23 Km², the third slope interval (10.6–15 degrees) covers an area of 5.17 Km², and the fourth slope interval (15.1–68 degrees) covers an area of 5.68 Km². It indicates that most areas of the Khurdopin glacier have favourable slopes. Through the slope variations with the LULC map for the year 2017 (Fig. 6), we observed that the

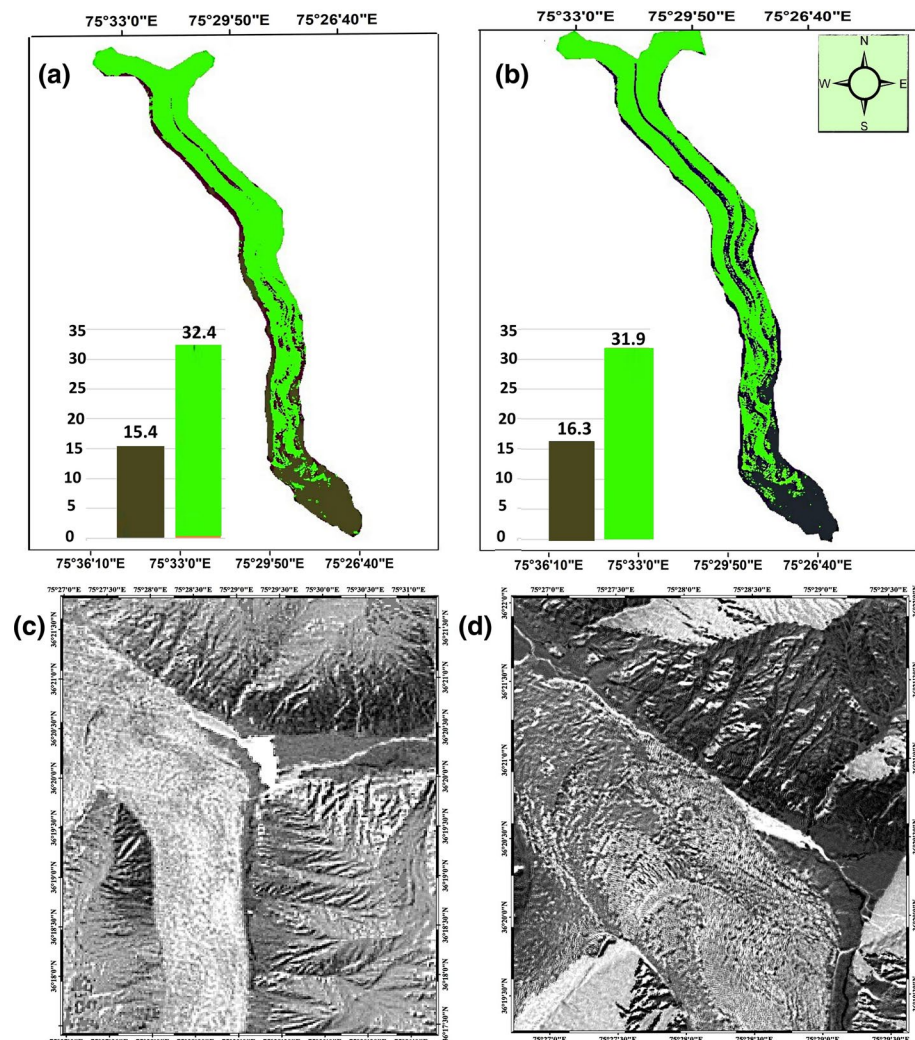


Fig. 7 Normalized snow difference index (NSDI) indicating the Khurdopin glacier debris (black) and snow covers (green) for the year 2000 (a), and 2017 (b); the normalized difference water index (NDWI) for the year 2000 (c) and 2017 (d)

glacier slope is steep in the accumulation and snout snow zones of the Khurdopin glacier, which is a favourable topographic combination for the surging of the glacier from the accumulation toward the ablation zone of the glacier.

Figure 8b shows the spatial variations of slope and aspect over the Khurdopin glacier, which are topographic parameters that describe the incoming solar radiation in a particular area. The aspect of the glacier surface includes flat (-1), North ($0^\circ\text{--}21.9^\circ$), Northeast ($22^\circ\text{--}66.9^\circ$), East ($67^\circ\text{--}111.9^\circ$), Southeast ($112^\circ\text{--}156.9^\circ$), South ($157^\circ\text{--}201.9^\circ$), Southwest ($202^\circ\text{--}246.9^\circ$), West ($247^\circ\text{--}291.9^\circ$), and Northwest ($292^\circ\text{--}336.5^\circ$) to North ($337^\circ\text{--}360^\circ$). East and Southeast slope aspects generally

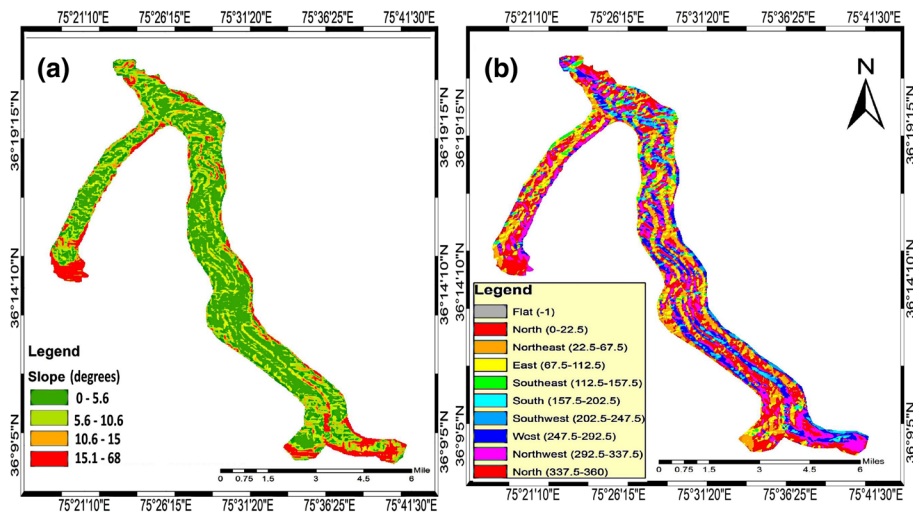


Fig. 8 Spatial variations of the Khurdopin glacier slopes (a) and slope-aspects (b)

receive more solar radiation first in the morning, when temperatures are usually cold-est. Moreover, it shows that the East, Flat, North, North East, North West, South, South East, South West, and West aspects cover an area of 0.10%, 0.02%, 0.24%, 0.22%, 0.18%, 0.03%, 0.03%, 0.05%, and 0.14%, respectively. North-facing aspects generally receive less heating energy. The 64% of the glacier slope aspects are north-facing, which receives more snowfall in the winter season, causing an increase in ice mass in the accumulation zone. Consequently, the resulting ice mass may generate a movement in the glacier towards the ablation zone.

3.6 Climatic changes over the Khurdopin glacier for the period 1999–2017

Figure 9a–b shows the LST maps of the Khurdopin glacier for the month of August in years 1999 Fig. 9a and 2017 Fig. 9b. They indicate that the minimum and maximum LST were -11°C and 21°C , respectively, in 2000. In 2017, the minimum and maximum LST were -13°C and 15°C , respectively. Figure 10 shows an increasing trend of the maximum temperature (Fig. 10a–d) and minimum temperature (Fig. 10e–h) from December to March for the period 1999–2017. There is a clear increasing temperature trend during the colder (winter) months in the Khurdopin glacier. This cold-temperature transition indicates favourable conditions for the high melting rate on the glacier, and, consequently, the increased pressure melting (Steiner et al. 2018). The melted water enters the glacier bed and acts as a lubricant, often causing the glacier movement.

Like temperatures, the mean annual precipitation from 1999 to 2017 shown in Fig. 9c indicates an increasing precipitation trend from 2009 onward. The snowfall trend in the Hunza basin decreases from November to January. This change in precipitation and snowfall patterns is a favourable condition causing a decrease in the glacier mass in the accumulation zone of the glacier (Sevestre and Benn 2015).

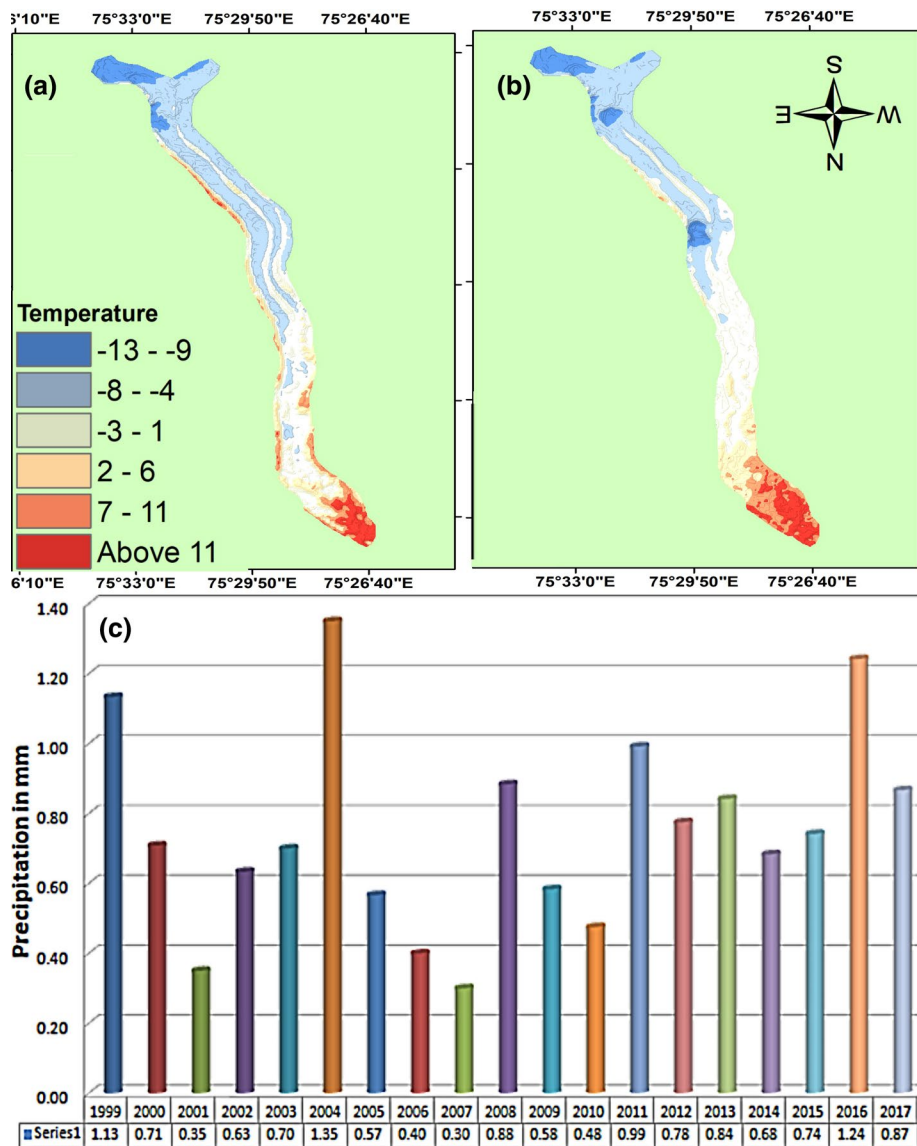


Fig. 9 Land surface temperature (LST) for August in the years 2000 (a) and 2017 (b); and the precipitation trend over the glacier from years 1999 to 2017

4 Discussions

The present study explains the topographic and climatic factors as possible drivers for the regular advancements on Khurdopin Glacier and the spatial and temporal variation in the Khurdopin glacier debris cover, snow cover, water bodies from the year 2000 to 2017. Moreover, these factors may explain the 4-year build-up time in both the 2017 and 1979 surges, in which the upper reach glacier surface increased with a decrease in the lower

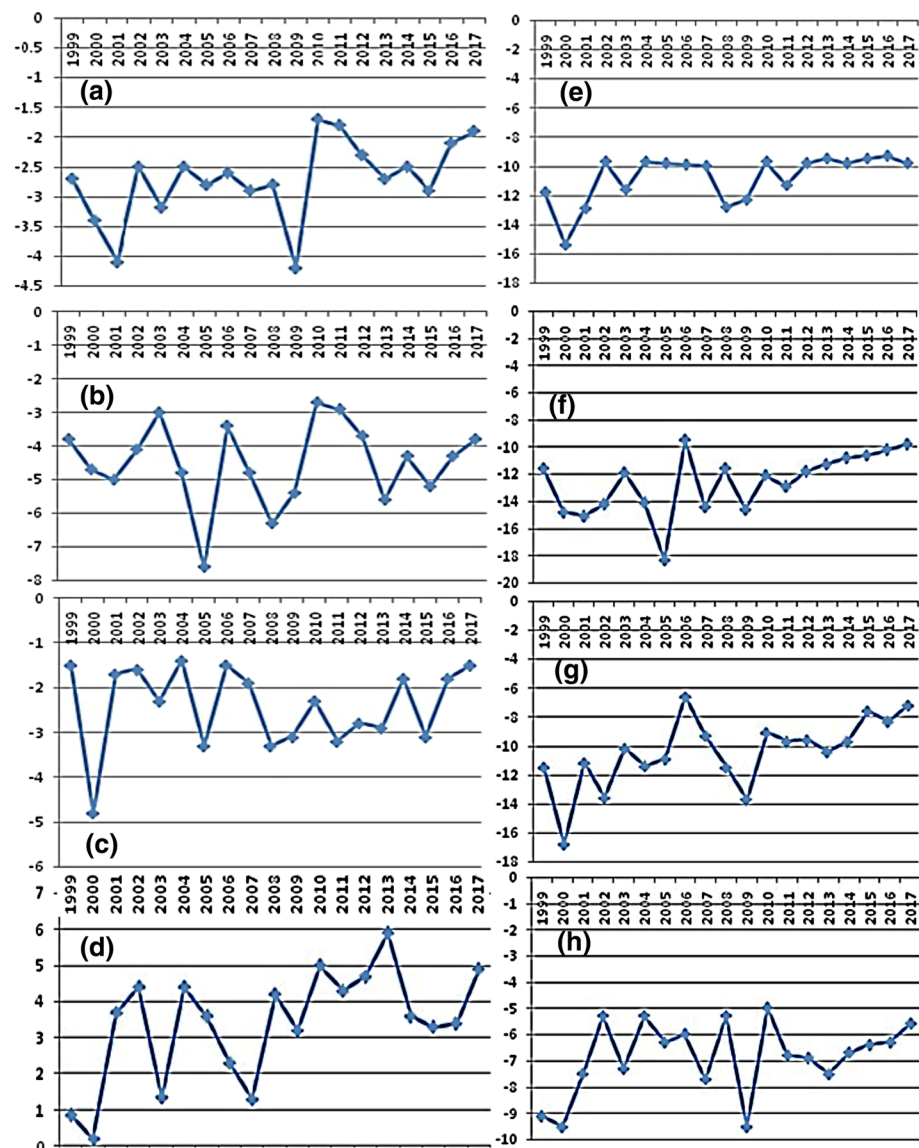


Fig. 10 Maximum temperature trend for December (a), January (b), February (c), and March (d); and, Minimum temperature trend for December (e), January (f), February (g), and March (h) from the year 1999 to 2017

reach (Steiner et al. 2018). Through comparing Figs. 7 and 8, we found 64% of the glacier aspect is north that receives more snowfall in the winter season, causing an increase in ice mass in the accumulation zone. Consequently, the resulting ice mass at the steep surface gradient may increase velocities in the glacier upper reaches towards the ablation zone. The increased velocities at a particular location may be triggered by temperature variations in glaciers and ice sheets, resulting in a rapid increase in the glacier sliding from 2015

Table 2 Statistics for the user's and the producer's accuracies of the land use land cover (LULC) classes in the classified imagery for the year 2017

LULC classes	User's accuracy (%)	Producer's accuracy (%)
Glacier	83.33	83.33
Debris cover	86.00	80.71
Mountains/barren land	91.52	88.23
Vegetation	99.33	100.00
Water	98.00	90.45
Fresh snow	94.00	88.12
Settlement	100.00	100.00
Overall accuracy	90.25%	
Kappa coefficient		0.891

The overall accuracy of 90.25% shows high classification accuracy, i.e., about 90% of assigned pixels are correctly assigned. The Kappa coefficient value 0.891 shows a strong level of agreement between classified and reference classes

onward. Moreover, overall all climatic parameters in this study indicate the favourable condition to influence the surging and melting of the Khurdopin glacier. We observed that the water bodies over the glacier cover vary with vegetation cover and soil types.

Our results show a total surge area of 0.27 Km² produced total glacial deposits of 6257688.99 cubic meters during the last Khurdopin surge on 23 May 2017. Moreover, this surge occurred at the start of the melting season. According to (Steiner et al. 2018), such a surge is often characterized to catalyze another surge when the glacial deposits reach the ice-bedrock interface. There is a continuous debate on the possible flow mechanisms to trigger the Khurdopin surge. However, most experts prefer the Basal sliding over the thermal shift (Kamb 1987; Quincey and Luckman 2014; Steiner et al. 2018). Our results based on remote sensing and field observations may provide further evidence to these processes. Future studies may use unmanned aerial vehicles (UAVs) to obtain detailed field observations in the targeted locations over small glacier areas. Moreover, the hyperspectral data can be obtained through short-range drone surveys. Such detailed data will help investigate the glacier surge processes related to the water-saturated granular-base material deformation (Damsgaard et al. 2015; Steiner et al. 2018).

Our results support previous studies on Khurdopin in witnessing a relatively consistent return period of a 20-year glacier surge from the end of the nineteenth century (Hewitt and Liu 2010; Quincey et al. 2011; Steiner et al. 2018). The Khurdopin recent surge is the fastest among all the reported glacier surges in the region, particularly compared to the recent surge in the neighbouring Hispar Glacier (Paul et al. 2017). During the latest glacier surge, the increased speed and redistribution of the ice volume mounted pressure on the glacier surface. Consequently, several crevasses that initially appeared during mid-May have been increased in both number and size since mid-July.

5 Conclusion

The present study investigates the advancement cycle of the Khurdopin glacier through remote sensing. In doing so, we tend to identify possible climatic and topographic factors that may influence glacier surging behaviour.

The spatio-temporal investigation of Landsat and ASTER images indicates the Khurdopin surge in the years 2000 and 2017. The recent surge blocked the Shimshal River that formed a glacier lake in the upstream area between Virjerab glacier and Khurdopin glacier. The recent glacier surge of the glacier initially started in October 2016 blocked approximately 2.3 Km length of the Shimshal River till 2017. This glacier was continuously blocking the river while the water drained through curves beneath the glacier. In 2000, it surged 0.69 km^2 areas while the glacial lake cover area was 0.52 km^2 . In the year 2017, the glacier blocked area was 0.62 km^2 area of the Shimshal River, and the glacial lake area was 0.38 km^2 . In the year 2000, the debris and fresh-snow cover areas of the Khurdopin glacier were 15.4 km^2 and 32.4 km^2 , respectively, while in 2017, these areas were changed to 16.3 km^2 and 39.1 km^2 , respectively.

We observed a temperature increase and spatial and temporal changes in snowfall patterns in the glacier accumulation zone from 2000 to 2017. Variations in the climatic variables co-occur with the steep glacier slopes on the north aspect that favour glacial surging. ASTER DEM data is suitable for the compilation of topographic parameters of the Khurdopin Glacier.

We conclude that the climatic and topographic environment of the Khurdopin glacier favours the glacier surging behaviour. The slope and aspect parameters are favourable for the glacier surge from the accumulation towards the ablation zone. The temporal variations in the climatic variables of precipitation and temperature also favour the movement of the glacier.

References

- Ashraf A, Naz R, Iqbal MB (2017) Altitudinal dynamics of glacial lakes under changing climate in the Hindu Kush, Karakoram, and Himalaya ranges. *Geomorphology* 283:72–79
- Awais M, Samin T, Gulzar MA, Hwang J (2019) The sustainable development of the China Pakistan economic corridor: synergy among economic, social, and environmental sustainability. *Sustainability* 11(24):7044
- Bajracharya SR, Maharjan SB, Shrestha F (2019) Glaciers in the Indus Basin. In: Indus River Basin, pages 123–144. Elsevier
- Bhambri R, Watson CS, Hewitt K, Haritashya UK, Kargel JS, Shahi AP, Chand P, Kumar A, Verma A, Govil H (2020) The hazardous 2017–2019 surge and river damming by Shispore Glacier, Karakoram. *Sci Rep* 10(1):1–14
- Chander G, Markham BL, Helder DL (2009) Summary of current radiometric calibration coefficients for Landsat MSS, TM, ETM+, and EO-1 ALI sensors. *Remote Sens Environ* 113(5):893–903
- Damsgaard A, Egholm DL, Piotrowski JA, Tulaczyk S, Larsen NK, Braendstrup C (2015) A new methodology to simulate subglacial deformation of water saturated granular material. *Cryosphere Discuss*. <https://doi.org/10.5194/tc-9-2183-2015>
- Fayaz A, ul Shafiq M, Singh H, Ahmed P (2020) Assessment of spatiotemporal changes in land use/land cover of North Kashmir Himalayas from 1992 to 2018. *Model Earth Syst Environ*. <https://doi.org/10.1007/s40808-020-00750-9>
- Fu X, Zhou J (2020) Recent surge behavior of Walsh Glacier revealed by remote sensing data. *Sensors* 20(3):716
- Gardelle J, Berthier E, Arnaud Y, Kaab A (2014) Region-wide glacier mass balances over the Pamir-Karakoram-Himalaya during 1999–2011. *The Cryosphere* 7:1263–1286

- Ge W, Cheng Q, Tang Y, Jing L, Gao C (2018) Lithological classification using sentinel-2a data in the shibanjing ophiolite complex in inner mongolia, China. *Remote Sens* 10(4):638
- Gilany N, Iqbal J (2020) Geospatial analysis and simulation of glacial lake outburst flood hazard in Shyok Basin of Pakistan. *Environ Earth Sci* 79(6):1–11
- Hewitt K, Liu J (2010) Ice-dammed lakes and outburst floods, Karakoram Himalaya: historical perspectives on emerging threats. *Phys Geogr* 31(6):528–551
- Imran M, Mahmood A (2020) Analysis and mapping of present and future drivers of local urban climate using remote sensing: a case of Lahore, Pakistan. *Arab J Geosci* 13(6):1–4
- Iturriaga L (2005) New observations on present and prehistorical glacier-dammed lakes in the Shimshal valley (Karakoram Mountains). *J Asian Earth Sci* 25(4):545–55
- Jiménez-Muñoz JC, Sobrino JA, Skoković D, Mattar C, Cristóbal J (2014) Land surface temperature retrieval methods from Landsat-8 thermal infrared sensor data. *IEEE Geosci Remote Sens Lett* 11(10):1840–1843
- Kamb B (1987) Glacier surge mechanism based on linked cavity configuration of the basal water conduit system. *J Geophys Res Solid Earth* 92(B9):9083–9100
- Nabi G, Ullah S, Khan S, Ahmad S, Kumar S (2018) China-Pakistan economic corridor (CPEC): melting glaciers? a potential threat to ecosystem and biodiversity. *Environ Sci Pollut Res* 25(4):3209–3210
- NASA-JPL (2018) Khurdopin Glacier, Pakistan
- Paul F (2015) Revealing glacier flow and surge dynamics from animated satellite image sequences: examples from the Karakoram. *The Cryosphere* 9(6):2201–2214
- Paul F, Strozzi T, Schellenberger T, Kääb A (2017) The 2015 surge of Hispar Glacier in the Karakoram. *Remote Sens* 9(9):888
- Pfeffer WT, Arendt AA, Bliss A, Bolch T, Cogley JG, Gardner AS, Hagen J-O, Hock R, Kaser G, Kienholz C et al (2014) The Randolph Glacier Inventory: a globally complete inventory of glaciers. *J Glaciol* 60(221):537–552
- Quincey D, Braun M, Glasser NF, Bishop M, Hewitt K, Luckman A (2011) Karakoram glacier surge dynamics. *Geophys Res Lett*. <https://doi.org/10.1029/2011GL049004>
- Quincey D, Luckman A (2014) Brief communication: on the magnitude and frequency of Khurdopin glacier surge events. *The Cryosphere* 8(2):571–574
- Quincey DJ, Glasser NF, Cook SJ, Luckman A (2015) Heterogeneity in Karakoram glacier surges. *J Geophys Res Earth Surf* 120(7):1288–1300
- Racoviteanu A, Williams MW (2012) Decision tree and texture analysis for mapping debris-covered glaciers in the Kangchenjunga area, Eastern Himalaya. *Remote Sens* 4(10):3078–3109
- Rashid I, Abdullah T, Glasser NF, Naz H, Romshoo SA (2018) Surge of Hispar Glacier, Pakistan, between 2013 and 2017 detected from remote sensing observations. *Geomorphology* 303:410–416
- Rashid I, Majeed U (2018) Recent recession and potential future lake formation on drang drung glacier, zanskar himalaya, as assessed with earth observation data and glacier modelling. *Environ Earth Sci* 77(12):429
- Rashid I, Majeed U, Jan A, Glasser NF (2020) The January 2018 to September 2019 surge of Shisper Glacier, Pakistan, detected from remote sensing observations. *Geomorphology* 351:106957
- Senese A, Maragno D, Fugazza D, Soncini A, D'Agata C, Azzoni RS, Minora U, Ul-Hassan R, Vuillermoz E, Asif Khan M, Shafiq Rana A (2018) Inventory of glaciers and glacial lakes of the Central Karakoram National Park (CKNP-Pakistan). *J Maps* 14(2):189–98
- Sevestre H, Benn DI (2015) Climatic and geometric controls on the global distribution of surge-type glaciers: implications for a unifying model of surging. *J Glaciol* 61(228):646–662
- Steiner JF, Kraaijenbrink PD, Jiduc SG, Immerzeel WW (2018) Brief communication: The Khurdopin glacier surge revisited-extreme flow velocities and formation of a dammed lake in 2017. *Cryosphere* 12(1):95–101
- USGS (2017) Khurdopin Glacier, Pakistan
- Veettil BK, Wang S, Simões JC, Pereira SFR (2018) Glacier monitoring in the eastern mountain ranges of Bolivia from 1975 to 2016 using landsat and sentinel-2 data. *Environ Earth Sci* 77(12):452
- Wang X-Y, Wang J, Jiang Z-Y, Li H-Y, Hao X-H (2015) An effective method for snow-cover mapping of dense coniferous forests in the upper Heihe river basin using landsat operational land imager data. *Remote Sens* 7(12):17246–17257
- Weng Q, Lu D, Schubring J (2004) Estimation of land surface temperature-vegetation abundance relationship for urban heat island studies. *Remote Sens Environ* 89(4):467–483
- Yan D, Huang C, Ma N, Zhang Y (2020) Improved landsat-based water and snow indices for extracting lake and snow cover/glacier in the tibetan plateau. *Water* 12(5):1339

- You QL, Ren GY, Zhang YQ, Ren YY, Sun XB, Zhan YJ, Krishnan R (2017) An overview of studies of observed climate change in the Hindu Kush Himalayan (HKH) region. *Adv Clim Chang Res* 8(3):141–147
- Zhang M, Chen F, Tian B, Liang D, Yang A (2020) Characterization of Kyagar Glacier and Lake Outburst Floods in 2018 Based on Time-Series Sentinel-1A Data. *Water* 12(1):184

Publisher's Note Springer Nature remains neutral with regard to jurisdictional claims in published maps and institutional affiliations.